sensors

MDPI

Article

Synthesis of Cu_2O-Modified Reduced Graphene Oxide for NO_2 Sensors

Manman Huang [1,2], Yanyan Wang [1,2,*], Shuyang Ying [1,2], Zhekun Wu [1,2], Weixiao Liu [1,2], Da Chen [3] and Changsi Peng [1,2]

[1] School of Optoelectronic Science and Engineering & Collaborative Innovation Center of Suzhou Nano Science and Technology, Soochow University, Suzhou 215006, China; 20195239010@stu.suda.edu.cn (M.H.); 20195239037@stu.suda.edu.cn (S.Y.); 20185208036@stu.suda.edu.cn (Z.W.); 20174208118@stu.suda.edu.cn (W.L.); changsipeng@suda.edu.cn (C.P.)

[2] Key Lab of Advanced Optical Manufacturing Technologies of Jiangsu Province & Key Lab of Modern Optical Technologies of Education Ministry of China, Soochow University, Suzhou 215006, China

[3] College of Electronics, Communications, and Physics, Shandong University of Science and Technology, Qingdao 266590, China; chenda@sdust.edu.cn

* Correspondence: author: yywang@suda.edu.cn

Abstract: Nowadays, metal oxide semiconductors (MOS)-reduced graphene oxide (rGO) nanocomposites have attracted significant research attention for gas sensing applications. Herein, a novel composite material is synthesized by combining two p-type semiconductors, i.e., Cu_2O and rGO, and a p-p-type gas sensor is assembled for NO_2 detection. Briefly, polypyrrole-coated cuprous oxide nanowires (PPy/Cu_2O) are prepared via hydrothermal method and combined with graphene oxide (GO). Then, the nanocomposite (rGO/PPy/Cu_2O) is obtained by using high-temperature thermal reduction under Ar atmosphere. The results reveal that the as-prepared rGO/PPy/Cu_2O nanocomposite exhibits a maximum NO_2 response of 42.5% and is capable of detecting NO_2 at a low concentration of 200 ppb. Overall, the as-prepared rGO/PPy/Cu_2O nanocomposite demonstrates excellent sensitivity, reversibility, repeatability, and selectivity for NO_2 sensing applications.

Keywords: reduced graphene oxide (rGO); cuprous oxide nanowires; polypyrrole; gas sensors; NO_2 sensing; p-type semiconductor

Citation: Huang, M.; Wang, Y.; Ying, S.; Wu, Z.; Liu, W.; Chen, D.; Peng, C. Synthesis of Cu_2O-Modified Reduced Graphene Oxide for NO_2 Sensors. *Sensors* **2021**, *21*, 1958. https://doi.org/10.3390/s21061958

Academic Editors: Sanli Faez, Peter Zijlstra and Filiz Yesilkoy

Received: 20 January 2021
Accepted: 2 March 2021
Published: 11 March 2021

1. Introduction

NO_2, as a major air pollutant, is responsible for acid rain and hazardous to human respiratory tracts. According to the World Health Organization (WHO), the safety limit for NO_2 gas is 410 ppb per hour [1]. Hence, monitoring the trace amounts of NO_2 is necessary from health perspective and plays an important role in environmental pollution [2], air quality, and industrial safety [3–7].

The two-dimensional graphene, discovered by Novoselov et al. in 2004 [8], is widely employed as a promising sensing material due to its high specific surface area (2.6×10^3 m^2/g) [9–13], ultra-high room-temperature electron mobility (2.0×10^5 cm^2/Vs), and chemical stability [14,15]. Additionally, graphene can be easily and cost-effectively prepared by a wide range of techniques, such as mechanical peeling [8], chemical vapor deposition [16,17], silicon carbide (SiC) epitaxial growth [18], redox method [19], and other methods. It has been reported that the changes in the external chemical environment result in significant differences in the sensing performance of graphene [20]. Schedin et al. have first reported the performance of graphene-based gas sensors in 2007 [21], however, the as-prepared sensors exhibited distinct disadvantages, such as slow as well as low response and poor selectivity [22,23].

Similar to graphene, metal oxides (MO) can also be used as sensing materials; however, MO-based sensors also possess some defects. The first MO-based commercial sensor appeared in the 1960s [24]. Moreover, the operating temperature of MO-based sensors ranges

from 150 to 400 °C and such a high operating temperature raises safety concerns, degrades device stability and reduces the operating life [22,25–30]. Some efforts have been made to achieve room-temperature sensing [24,31]. Currently, graphene-based nanocomposites are the focus of research for sensing applications [32–35]. In particular, MO-graphene nanocomposites have garnered intensive attention because of their excellent sensing properties [14]. Cu_2O, as a typical p-type semiconductor, is a promising candidate among different metal oxides. Different morphologies of Cu_2O, such as spherical, rod-like, lamellar, and tubular, have been studied for sensing applications [36–40]. It is expected that the incorporation of Cu_2O between graphene nanosheets can enlarge the specific surface area, increase active sites and enhance the adsorption capacity of graphene, improving the affinity for gas molecules. Additionally, the presence of Cu_2O can prevent the restacking of graphene sheets and overcome inferior gas selectivity of graphene [41,42].

Compared with common polymers, conductive polymers possess a unique unlocalized conjugated π-electron system [43]. The long-range conjugation not only greatly reduces the gap between the bonding and antibonding bands, but also widens the distance between two bands. It increases the number of orbitals in the band and reduces the gap between orbitals, allowing the free movement of carriers within the band. Polypyrrole (PPy), as an important conductive polymer [44], renders high chemical stability, high conductivity, redox reversibility, good dispersion, simple preparation, and low cost [45,46], showing great potential in sensing applications [46]. By introducing PPy into graphene-based materials, the electrostatic repulsion between PPy nanoparticles can effectively prevent the accumulation of graphene sheets, optimizing the sensing properties of graphene-based materials.

The comparison of NO_2 sensors, based on reduced graphene oxide (rGO) or Cu_2O composites, reveals that designing and fabricating sensing devices based on binary or ternary components with excellent sensing properties is still a challenge (Table 1) [12,14]. Hence, in this work, graphene-polypyrrole-coated copper oxide nanowires ternary components were designed and prepared for room temperature for sensing applications. The PPy/Cu_2O were easily formed by the hydrothermal method using pyrrole as templates. Further assembly of graphene oxide (GO) with PPy/Cu_2O and reduction were carried out to form ternary components by optimizing the preparation conditions, where the micro- and nanoscale of each component was regulated and combined with the optimal composite ratio to obtain the composite nanomaterials with specific properties. Moreover, the synergistic reinforcement between different components leads to optimal performance. In general, the as-prepared gas sensors via assembly techniques realize room-temperature sensing. These sensors exhibit a maximum NO_2 response of 42.5% and are capable of detecting NO_2 at a low concentration of 200 ppb. In addition, the sensors show excellent repeatability and selectivity.

Table 1. The comparison of various NO_2 sensors based on rGO and Cu_2O composites.

Material	Response	Concentration	Working Temperature	Reference
SnO_2/graphene	0.25 ($\Delta R/R_a$)	10 ppm	Room temperature	[6]
rGO-SnO_2	53.57 (R_g/R_a)	3 ppm	125 °C	[22]
SnS_2-rGO	9.8% ($\Delta R/R_a$)	0.6 ppm	80 °C	[27]
rGO/In_2O_3	22.3 (R_g/R_a)	500 ppb	150 °C	[28]
$BiVO_4$/Cu_2O	4.2 (R_g/R_a)	4 ppm	60 °C	[29]
$BiVO_4$/Cu_2O/rGO	8.2 (R_g/R_a)	1 ppm	60 °C	[30]
Au/Cu_2O/ZnO	26% ($\Delta R/R_a$)	5 ppb	Room temperature	[31]
MoS_2/graphene	69% ($\Delta R/R_a$)	10 ppm	200 °C	[33]

2. Experimental

2.1. Materials

All chemical reagents were of analytical grade and used as received without further purification. Pyrrole, acetic acid, ethanol, acetone, concentrated sulphuric acid, and hydrogen peroxide were purchased from the Sinopharm Chemical Reagent Co., Ltd., Shanghai, China. Copper acetate monohydrate was obtained from the Gretel Pharmaceutical Technology Co., Ltd., Suzhou, China.

2.2. Synthesis of Polypyrrole-Coated Cu_2O Nanowires

PPy-coated Cu_2O nanowires were prepared by a one-step hydrothermal method [47,48], where copper acetate monohydrate was used as a precursor and pyrrole acted as a reducing and structure-directing agent under weak acidic conditions. Initially, 0.2 g of copper acetate monohydrate were added in a certain amount of deionized water and ultrasonicated for 5–10 min for complete dissolution. Then, the pyrrole monomer (0.075 mL) was added into a small amount of deionized water. After transient ultrasonication, it was slowly added to the above solution and stirred with a glass rod. Then, 0.15 mL of acetic acid (1 mol/L) was added to the above mixture to make sure the dissolution of pyrrole monomers. The resulting mixture was transferred to an autoclave and placed in an oven at 120 °C for 12 h. Finally, the reaction solution was cooled down to room temperature and polypyrrole-coated copper oxide nanowires were obtained by sequentially washing with deionized water, ethanol, and acetone, followed by filtration and drying. The hydrothermal temperature of 120, 140, and 160 °C was also used to investigate the influence of growth temperature on structure and morphology.

2.3. Preparation of rGO/PPy/Cu_2O Nanocomposites

GO was prepared by the modified Hummers method [49]. First, a certain amount of PPy/Cu_2O nanowires was added into ethanol and ultrasonicated for 30 min to obtain a concentration of 2 mg/mL. A certain amount of 2 mg/mL GO solution was added into the above solution, ultrasonicated for 30 min and magnetically stirred for 3–5 h. Finally, the completely dispersed and uniformly mixed solution was filtered, washed, and dried to obtain GO/PPy/Cu_2O nanocomposite. The as-prepared GO/PPy/Cu_2O nanocomposites were placed in a tube furnace and heated at 350 °C for 1 h under the protection of Ar gas, resulting in the reduction in GO and formation of rGO/PPy/Cu_2O nanocomposites.

2.4. Fabrication of rGO/PPy/Cu_2O-Based Gas Sensor

Herein, the interdigitated electrode for gas sensing was prepared by the lift-off process [13]. First, a silicon wafer was heated at 90 °C in a mixture of concentrated H_2SO_4 and H_2O_2 for a certain time to obtain a hydrophilic silicon substrate. Then, the photoresist was applied to the silicon substrate. After a series of operations, we have obtained the planar interdigital electrodes by using the self-designed mask plate after exposure, sputtering and peeling. The as-prepared rGO/PPy/Cu_2O nanocomposite was ultrasonically dispersed in ethanol to obtain a suspension with a concentration of 1 mg/mL. The same amount of dispersion was measured by a micropipette and applied to the interdigital electrode. The two poles of the interdigital electrode were connected through the gas sensing material. To observe it visually, SEM characterization of the device is shown in Figure 1. Finally, the as-prepared sensor was vacuum-dried before further characterization.

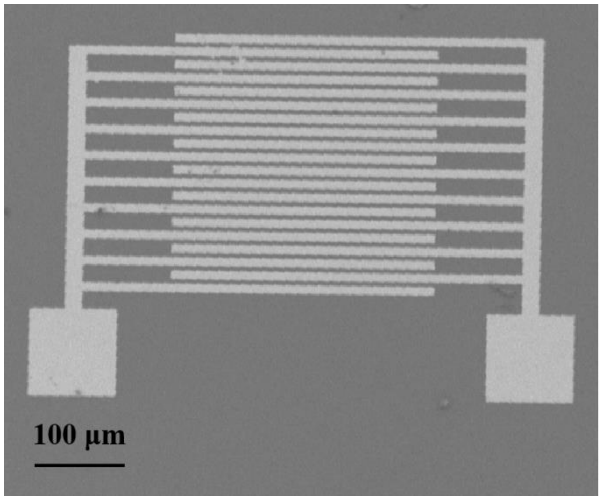

Figure 1. SEM image of the tested device.

2.5. Gas Sensor Sensitivity

In order to simulate the real detection environment, we have utilized compressed air as a background and dilution gas during the gas sensitivity test. The test temperature was set at 25 °C and mild test conditions were used, which are comparable to the practical applications. Figure 2 shows a sketch of the gas sensing set-up. Prior to the test, the background gas was introduced for a certain time to remove the residual exhaust gas from the gas path. Then, the desired concentration of NO_2 gas was introduced at the beginning of the test. The NO_2 concentration (C_N) can be given as:

$$C_N = \frac{5000 \times F_N}{F_N + F_C} \quad (1)$$

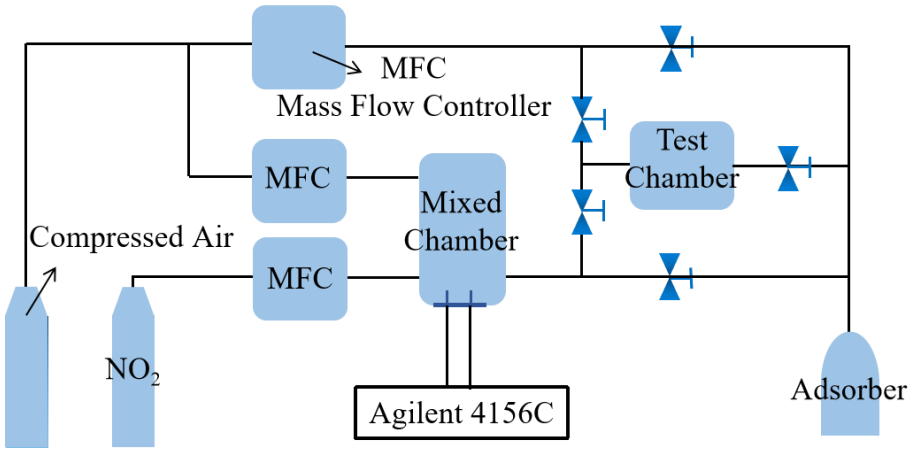

Figure 2. Schematic illustration of the gas sensing system.

The concentration of the NO_2 cylinder was 5000 ppm. F_N (sccm) refers to the flow rate of the NO_2 gas and F_C (slm) represents the flow rate of diluted gas (air).

When NO_2 gas passed through the sensor, the hole concentration of as-prepared rGO/PPy/Cu_2O nanocomposite increased and the resistance decreased due to the adsorption between NO_2 gas and as-prepared rGO/PPy/Cu_2O nanocomposite. The gas sensitivity (S, %) can be calculated from the change in resistance using the I-T curve, as given below:

$$S(\%) = \frac{R_g - R_a}{R_a} \times 100\% = \frac{\Delta R}{R_a} \times 100\% \quad (2)$$

where R_a represents the resistance of sensor in air and R_g corresponds to the resistance after the introduction of the NO_2 gas.

3. Results and Discussion

3.1. Characterization of as-Prepared Nanocomposites

Scanning electron microscopy (SEM) is employed to explore the influence of different growth temperatures on the morphology and microstructure of PPy/Cu_2O nanowires. As shown in Figure 3a, the length of copper oxide nanowires, grown at 120 °C, ranges from tens to hundreds of microns. Additionally, a smooth surface with uniform thickness is achieved (Figure 3b). However, when the growth temperature is increased to 140 °C, the copper oxide nanowires started to bend and exhibited different lengths (Figure 3c). One should note that the shorter copper oxide nanowires are not desirable for subsequent preparation of conductive films. As shown in Figure 3d, the further increase in growth temperature to 160 °C resulted in shorter copper oxide nanowires. Hence, the lower growth temperature is more favorable for copper oxide nanowires. One should also note that the growth temperature of <120 °C is not sufficient to produce copper oxide nanowires. In addition, Cu_2O with a completely linear structure can be obtained at these reaction temperatures.

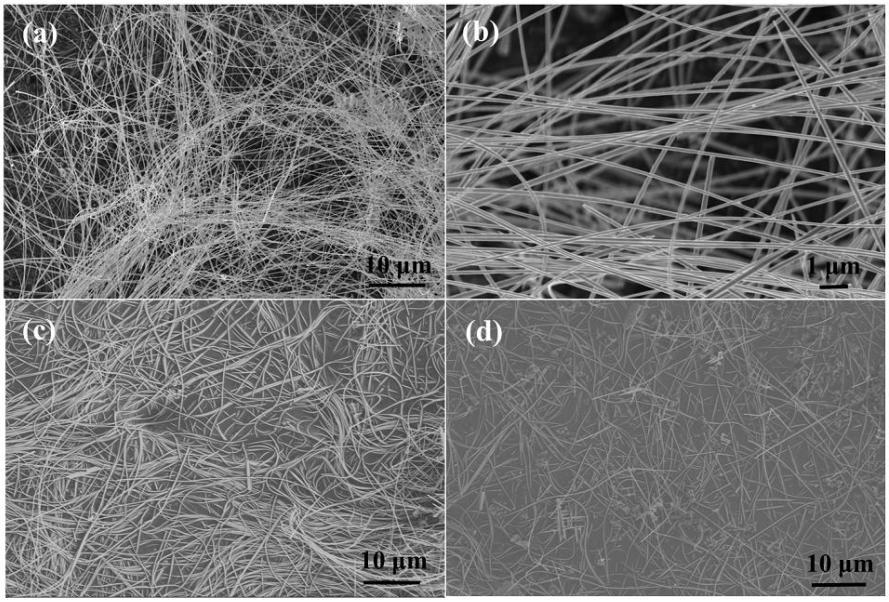

Figure 3. SEM images of hydrothermally-prepared PPy/Cu_2O nanowires at different temperatures: (**a**,**b**) 120 °C; (**c**) 140 °C; and (**d**) 160 °C.

Furthermore, the graphene content also influences the morphology of resulting nanocomposites. It can be readily observed that graphene facilitates the recombination and coating of PPy/Cu_2O nanowires. On the other hand, the excessive amount of graphene leads to the stacking of graphene sheets, which is highly undesirable for sensing applications. SEM is utilized to observe the morphology and microstructure of as-prepared rGO/PPy/Cu_2O nanocomposites (Figure 4). Overall, the utilization ratio of graphene increased with increasing graphene content in as-prepared rGO/PPy/Cu_2O nanocomposites. However, the excess of graphene will decrease the exposure of PPy-coated Cu_2O nanowires and result in uneven dispersion and stacking of graphene sheets.

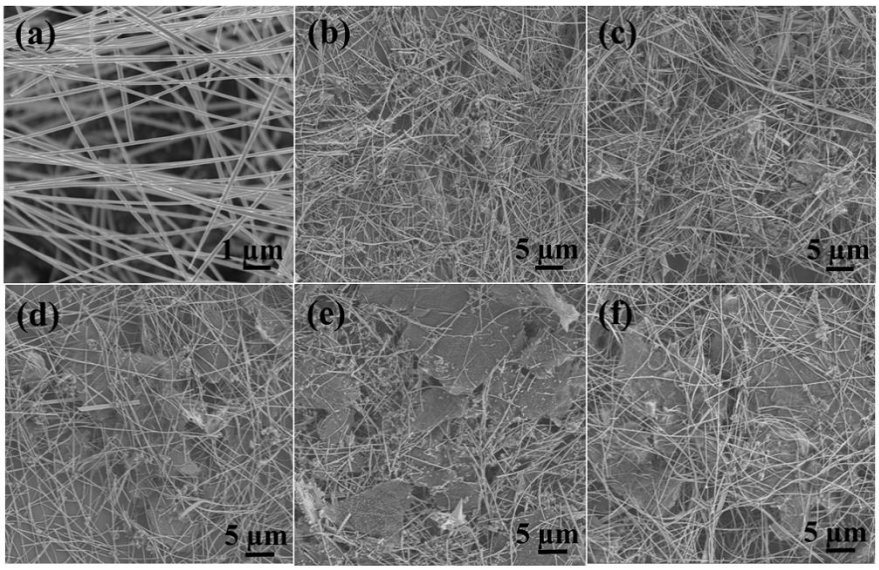

Figure 4. (**a**) SEM image of PPy-coated Cu_2O nanowires, hydrothermally prepared at 120 °C, and as-prepared rGO/PPy/Cu_2O nanocomposites after high-temperature thermal reduction. The GO to PPy/Cu_2O mass ratio is (**b**) 0.08, (**c**) 0.1, (**d**) 0.12, (**e**) 0.15, and (**f**) 0.20.

The structure of as-prepared nanocomposites was confirmed by X-ray diffraction (XRD). Figure 5 confirms the existence of Cu_2O and graphene characteristic peaks. Herein, the diffraction peaks at 2θ = 29.5°, 36.4°, 42.2°, 61.3°, and 73.5° correspond to (110), (111), (200), (220), and (311) planes of the Cu_2O (JCPDS card no. 05-0667) [50,51]. In the XRD patterns of three hybrid structures, we can clearly see the diffraction peaks of Cu_2O and the (111) and (200) peaks exhibit a relatively high intensity. Similarly, the characteristic diffraction peaks of graphene oxide and reduced graphene oxide are observed at 2θ = 10.2° and 23.1°, respectively. Since the relative quantity of Cu_2O is much higher than rGO, the diffraction peaks of Cu_2O are significantly stronger than the rGO. In addition, we have not observed phases other than rGO and Cu_2O. These results confirm that the rGO/PPy/Cu_2O nanocomposites have been successfully prepared after high-temperature reduction.

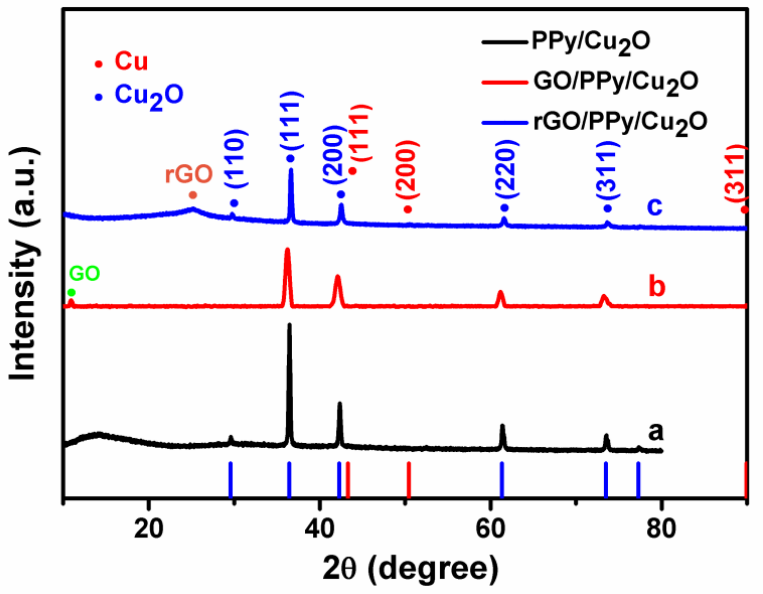

Figure 5. XRD patterns of (a) PPy-coated Cu_2O, (b) GO/PPy/Cu_2O nanocomposites and (c) rGO/PPy/Cu_2O nanocomposites.

Moreover, Raman spectroscopy is carried out to confirm that the graphene oxide is successfully transformed into the reduced graphene oxide (rGO) [52–55]. Figure 6 shows two characteristic Raman peaks at 1333 and 1582 cm^{-1}, corresponding to D- and G-bands, respectively. The D-band is related to defect scattering and electron/hole recombination during oxidation and reduction processes. Overall, the intensity of D-band represents the degree of disorder in graphene. On the other hand, the G-band is related to the bond stretching of all pairs of sp^2 atoms, indicating the integrity of sp^2 hybridized structure. In general, the reduction in graphene is analyzed by measuring the intensity ratio of D- to G-bands (I_D/I_G).

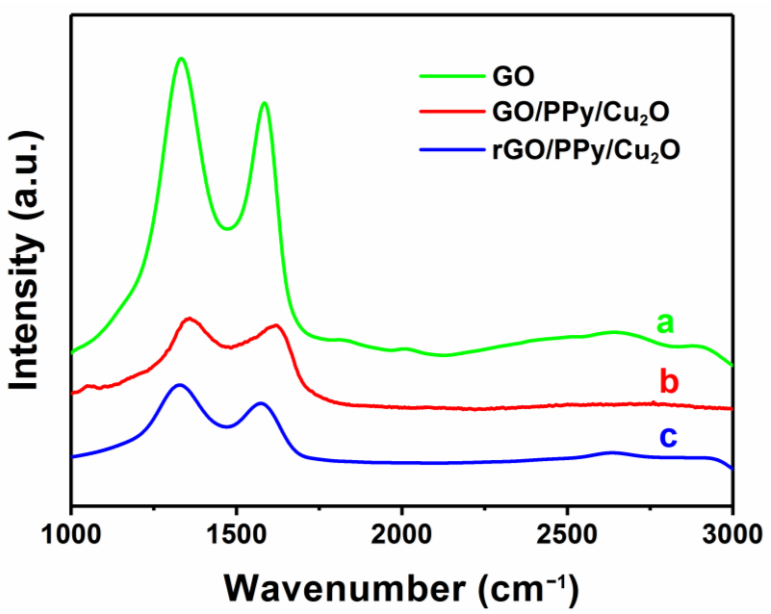

Figure 6. Raman spectra of (a) GO, (b) GO/PPy/Cu_2O and (c) rGO/PPy/Cu_2O.

Figure 6 exhibits that the ID/IG ratio of GO/PPy/Cu_2O and rGO/PPy/Cu_2O nanocomposite is 1.133 and 1.153, respectively. Theoretically, when GO is reduced, the oxygen-containing functional groups on the graphene sheets are removed [56], the ordering of sp^2 carbon network structure is increased, sp^2 region is widened and the ID/IG ratio is decreased. In fact, a large number of sp^3 hybridized carbon atoms deoxidize to form a new sp^2 hybridized region, and the re-formed sp^2 region is smaller than GO, minimizing the average sp^2 region of rGO, which is reflected by the enhancement of ID/IG. To further illustrate the successful fabrication of rGO/PPy/Cu_2O nanocomposites, we have employed Fourier transform infrared spectroscopy (FTIR) to characterize the changes in functional groups before and after high-temperature thermal reduction (Figure 7). The absorption peak near 3250 cm^{-1} can be attributed to N-H stretching vibrations of PPy and O-H stretching vibrations of GO. The absorption peak at 1552 cm^{-1} can be assigned to the vibrations of C=C skeleton, whereas the absorption peaks at 1323 and 1074 cm^{-1} can be attributed to the stretching vibrations of C-N, confirming the existence of PPy in as-prepared rGO/PPy/Cu_2O nanocomposites. In the case of GO/PPy/Cu_2O nanocomposite, the absorption peaks at 1625 and 1716 cm^{-1} correspond to the vibrational absorption of -COOH and C=O in carboxylic acids, respectively. One should note that the absorption intensity of -COOH and C=O groups in the FTIR spectrum of rGO/PPy/Cu_2O nanocomposites is weakened, whereas the absorption peak of C-O at 1040 cm^{-1} is disappeared, indicating the reduction in oxygen-containing functional groups from the graphene surface and confirming the successful transformation of GO into rGO.

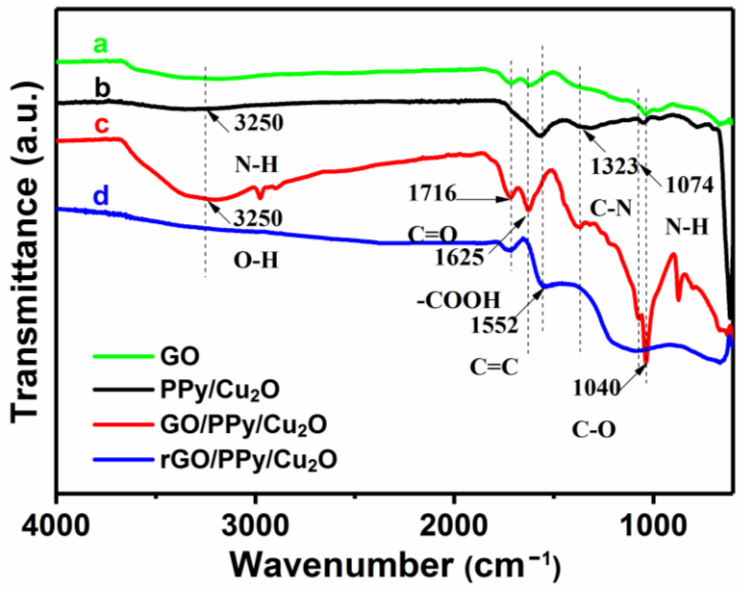

Figure 7. FTIR spectra of (a) GO, (b) PPy-coated Cu_2O nanowires, (c) GO/PPy/Cu_2O and (d) rGO/PPy/Cu_2O nanocomposites.

Furthermore, we have utilized X-ray photoelectron spectroscopy (XPS) to qualitatively analyze the elemental composition of as-prepared rGO/PPy/Cu_2O nanocomposites. Figure 8 shows the wide-range and high-resolution C 1s XPS spectra of GO and rGO/PPy/Cu_2O. The characteristic peaks of C-C/C=C (284.6 eV), C-O (286.9 eV), C=O (287.8 eV), and COOH (289.0 eV) can be clearly observed in the high-resolution C 1s spectrum (Figure 8b) [57]. The characteristic peak of C-N (285.5 eV) is observed in the high-resolution C 1s spectrum of the as-prepared rGO/PPy/Cu_2O nanocomposite (Figure 8d). Compared with the graphene oxide, the intensity of C-O, C=O, and COOH peaks is weakened in rGO/PPy/Cu_2O nanocomposites due to the high-temperature thermal reduction in GO.

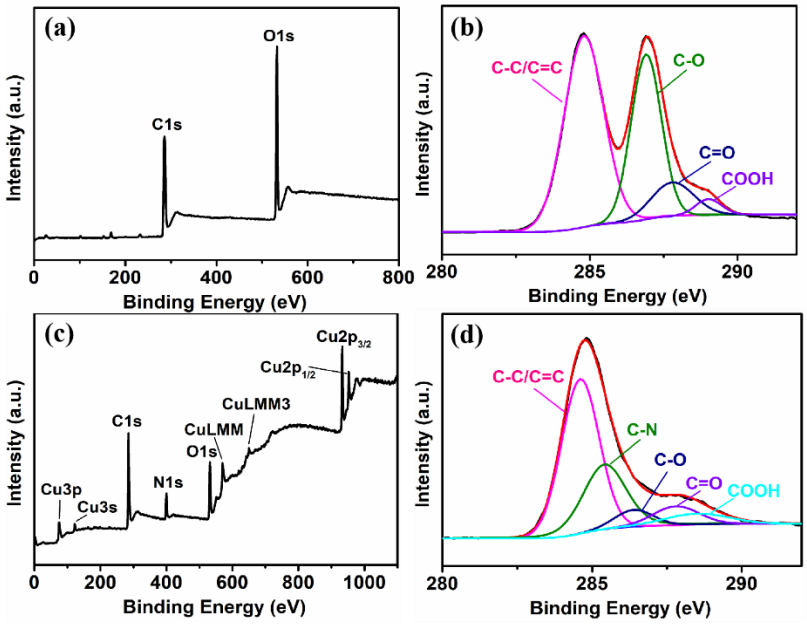

Figure 8. XPS spectra of rGO/PPy/Cu_2O nanocomposite before and after high-temperature thermal reduction: (**a**) wide-range and (**b**) high-resolution C 1s XPS spectra of GO, and (**c**) wide-range and (**d**) high-resolution C 1s XPS spectra of rGO/PPy/Cu_2O nanocomposites.

Overall, SEM, XRD, Raman spectroscopy. FTIR and XPS confirm the successful synthesis of rGO/PPy/Cu_2O nanocomposites, confirming the elemental composition and structure.

Figure 9 presents the response curves of PPy-coated Cu_2O nanowires sensor and rGO/PPy/Cu_2O nanocomposite sensors, with different graphene contents, to NO_2 flow of 50 ppm. The mass ratio of GO to PPy/Cu_2O nanowires was set at 0.08, 0.1, 0.12, 0.15, and 0.2, and the resulting rGO/PPy/Cu_2O nanocomposites are named as D_0, E_0, F_0, G_0, and J_0, respectively. Herein, the resistance response reached the maximum value within 300 sec after the introduction of NO_2 gas. The gas-sensitive response values of D_0, E_0, F_0, G_0, and J_0 were found to be 25.0, 42.5, 35.9, 30.0, and 25.1%, respectively. The ratio of 0.1 composite presents a maximum response, which is about 2.7 times of the sensor based on pure PPy-coated Cu_2O nanowires (15.7%). Additionally, the sensor recovered the initial resistance level after ≈200 sec under the auxiliary irradiations of an ultraviolet lamp. The experimental results reveal that the rGO/PPy/Cu_2O-based sensor renders superior gas sensing response, reaching the maximum response value of 42.5% at GO content of E_0. The further increase in graphene content leads to restacking of graphene sheets and loss of excellent graphene properties, resulting in an inferior gas sensing response.

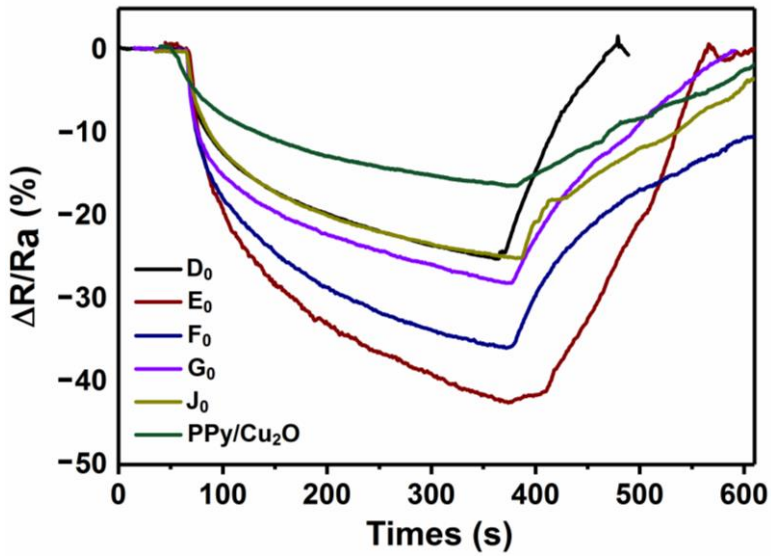

Figure 9. The gas sensing response curves of rGO/PPy/Cu_2O nanocomposites with different mass ratios of GO to PPy/Cu_2O nanowires to the NO_2 flow of 50 ppm (D_0: 0.08; E_0: 0.1; F_0: 0.12; G_0: 0.15; and J_0: 0.20).

As graphene content of 0.1 (E_0) endows superior gas sensing properties to the as-prepared rGO/PPy/Cu_2O nanocomposite, we have evaluated the sensing efficiency of E_0-based gas sensor under different concentrations of NO_2 (Figure 10). The NO_2 concentration of 50, 5, 1 ppm, 500 ppb, and 200 ppb resulted in the response value of 44.0, 38.0, 32.7, 24.4, and 20.3%, respectively. Under different gas concentrations, the quick response time of E_0 is ≈ 300 s and the recovery time can be reduced to ≈150–200 s under auxiliary irradiation of UV lamp [6]. One should note that the E_0-based gas sensor rendered excellent gas sensing response at low NO_2 concentrations, which indicates the superior NO_2 adsorption effect of the as-prepared rGO/PPy/Cu_2O nanocomposite, resulting in adsorption saturation in a relatively small time and high gas sensitivity. The sensor response with respect to NO_2 concentration is mainly nonlinear [58,59] because of the Langmuir adsorption of NO_2 on the surface of active substance. As the concentration of the target gas increases, the adsorption reaches saturation level and results in a decrease in response.

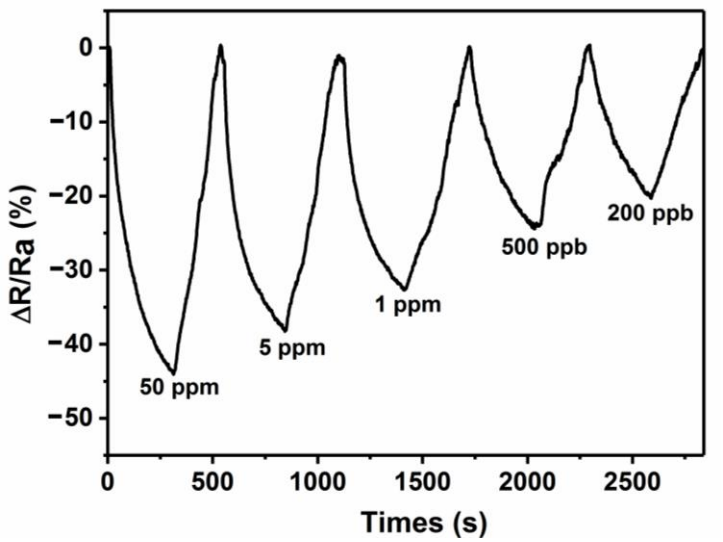

Figure 10. The gas response curves of E_0-based gas sensor under different NO_2 concentrations.

From a practical viewpoint, sustainable reuse is of great significance for gas sensors. Figure 11 shows the repeated gas sensing response evaluation of the E_0-based gas sensor at NO_2 flow of 50 ppm, showing excellent repeatability with one cycle consisting of almost 600 s. First of all, the response reaches the saturation level after 300 s of NO_2 gas injection. Then, the NO_2 gas is turned-off and background gas is turned-on at the same time. Under the illumination of ultraviolet lamp, NO_2 gas is gradually desorbed and blown away by air. The sensor begins to gradually recover the initial resistance level. In this way, three cycles of cyclic testing are carried out to detect the repeatability of the E_0-based gas sensor. Figure 11 confirms that the gas sensing response of the E_0-based sensor at 50 ppm of NO_2 gas is stable at ~43.0%. After three cycles, the response sensitivity does not decrease significantly, which further confirms that the as-prepared E_0-based gas sensor possesses excellent response stability and repeatability. Under normal usage conditions, the GO/PPy/Cu_2O-based gas sensor demonstrates excellent stability with only a slight decline in the response of 1.5% after 30 days, indicating good long-term stability.

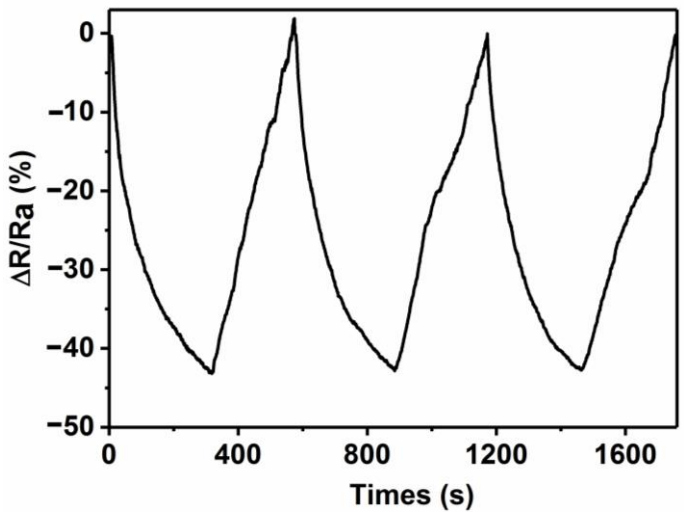

Figure 11. The repeatability and cyclic stability of the E_0-based gas sensor.

Furthermore, it is of utmost importance to assess the selectivity of adsorbed gas in practical applications. Therefore, we have investigated the adsorption of different industrial and laboratory gases, such as chloroform, formaldehyde, ethanol, acetone, and ethyl acetate, by the E_0-based gas sensor. The saturation vapor pressure of 1% is obtained by the bubbling

method and the response of NO_2 gas (50 ppm) is used as a comparison point to assess sensor selectivity (Figure 12). Figure 12 shows that the response of E_0-based sensor to other gases is extremely low. For instance, formaldehyde exhibited the highest response of 2.5% among the tested gases, which is much lower than the response of 50 ppm NO_2 gas (42.5%). One should note that the concentration of these gases is much higher than 50 ppm. Still, the E_0-based sensor demonstrated superior selectivity to the NO_2 gas.

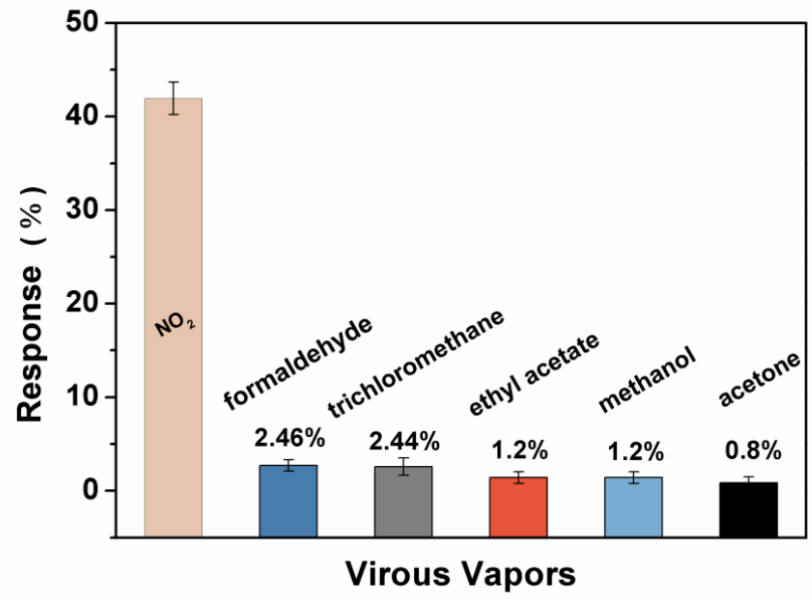

Figure 12. The selectivity of E_0-based sensor.

3.2. Sensing Mechanism

Cu_2O, rGO, and PPy have similar p-type nature [37,60]. When the composite material is exposed to air, O_2 molecules could be adsorbed on the material surface in the form of adsorbed

$$O_2(gas) + e^- \rightarrow O_2^-(ads) \quad (3)$$

After the introduction of NO_2, NO_2 molecules could be directly adsorbed on the surface by capturing electrons from the material (Equation (4)). In addition, NO_2 also gains electrons from adsorbed oxygen ions (Equation (5)).

$$NO_2(gas) + e^- \rightarrow NO_2^-(ads) \quad (4)$$

$$NO_2(gas) + O_2^-(ads) + 2e^- \rightarrow NO_2^-(ads) + 2O^- \quad (5)$$

Figure 13 illustrates the gas sensing mechanism. After the above process [61], the hole concentration of the device increases. Herein, p-type polypyrrole completes the process of doping and de-doping by gas adsorption and desorption, respectively [62,63]. Meanwhile, graphene and polypyrrole provide a large number of binding sites for gas adsorption. The high charge mobility of conducting polymer, i.e., polypyrrole, and graphene facilitates carrier transport and migration to the electrode for collection. These processes lead to the rapid decrease in electron concentration within the rGO/PPy/Cu_2O composites. In general, hole-assisted carrier transport is responsible for the conduction of p-type semiconductors. The hole concentration significantly increases with the decrease in electron concentration in rGO/PPy/Cu_2O composite due to NO_2 adsorption, which increases sensor conductivity.

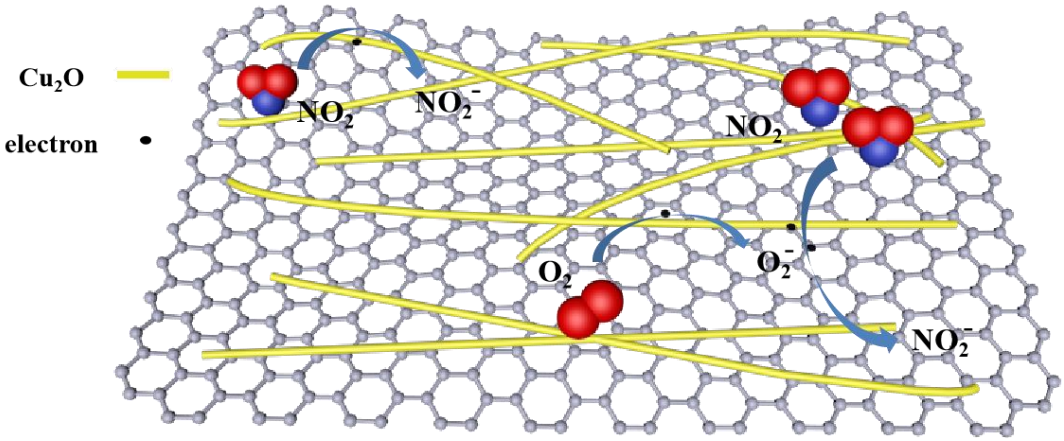

Figure 13. Schematic illustration of the NO_2 sensing mechanism of rGO/PPy/Cu_2O-based sensor.

According to the principle of complementary feedback of gas sensor [64], the combination of p-type semiconductors in gas sensors renders a synergistic influence on gas sensing characteristics and temperature coefficients of both materials, reducing zero drift, shortening initial relaxation time, and rendering superior selectivity and stability. Herein, the interdigital electrode is equivalent to the parallel connection of a sensor and several resistors, which reduces the initial resistance of the sensor. The decrease in initial resistance of sensor increased the change in resistance, which corresponds to the response value. During the recovery stage of gas sensor, the newly adsorbed air molecules eliminate residual NO_2 molecules from the surface of rGO/PPy/Cu_2O nanocomposite by introducing air and auxiliary irradiations under an ultraviolet lamp [65], increasing the resistivity of p-type semiconductor and recovering to the initial resistance.

4. Conclusions

In summary, PPy-coated Cu_2O nanowires have been prepared by the hydrothermal reaction and combined with graphene oxide to obtain rGO/PPy/Cu_2O nanocomposites after high-temperature thermal reduction. Moreover, a p-p-type gas sensor has been fabricated using rGO/PPy/Cu_2O nanocomposite as an electrode and room temperature sensing is realized. The results revealed that the rGO/PPy/Cu_2O-based gas sensor renders better NO_2 sensing performance than the PPy/Cu_2O-based sensor, confirming the positive influence of graphene addition. When the mass ratio of graphene to PPy-coated Cu_2O nanowires was 0.1, the rGO/PPy/Cu_2O-based sensor demonstrated the highest response value of 42.5% for NO_2 gas (50 ppm). When the concentration of NO_2 was as low as 200 ppb, the rGO/PPy/Cu_2O-based sensor still exhibited a response value of 20.3%. Moreover, the rGO/PPy/Cu_2O-based sensor has also rendered stable repeatability and excellent selectivity at the NO_2 concentration of 50 ppm.

Author Contributions: Conceptualization, writing-review and editing, project administration, Y.W.; Writing-original draft preparation, data curation, M.H.; methodology, validation, resources, Y.W. and D.C.; project design, supervision, Y.W. and C.P.; investigation, experiment test, Z.W. and W.L.; chart preparation, S.Y.; device fabrication, W.L. All authors have read and agreed to the published version of the manuscript.

Funding: This research was funded by the National Natural Science Foundation of China (Grant No. 61871281, 51,302,179 and 61574086), the International Cooperation Project by MOST of China (SQ2018YFE010343), and the Priority Academic Program Development (PAPD) of Jiangsu Higher Education Institutions.

Institutional Review Board Statement: Not applicable.

Informed Consent Statement: Not applicable.

Data Availability Statement: Not applicable.

Acknowledgments: The authors gratefully acknowledge financial support from the National Natural Science Foundation of China (Grant No. 61871281, 51,302,179 and 61574086), the International Cooperation Project by MOST of China (SQ2018YFE010343), and the Priority Academic Program Development (PAPD) of Jiangsu Higher Education Institutions.

Conflicts of Interest: The authors declare no conflict of interest.

References

1. Zhou, Y.; Liu, G.; Zhu, X.; Guo, Y. Cu_2O quantum dots modified by RGO nanosheets for ultrasensitive and selective NO_2 gas detection. *Ceram. Int.* **2017**, *43*, 8372–8377. [CrossRef]
2. Giancaterini, L.; Cantalini, C.; Cittadini, M.; Sturaro, M.; Guglielmi, M.; Martucci, A.; Resmini, A.; Anselmi-Tamburini, U. Au and Pt Nanoparticles Effects on the Optical and Electrical Gas Sensing Properties of Sol–Gel-Based ZnO Thin-Film Sensors. *IEEE Sens. J.* **2015**, *15*, 1068–1076. [CrossRef]
3. Impeng, S.; Junkaew, A.; Maitarad, P.; Kungwan, N.; Zhang, D.; Shi, L.; Namuangruk, S. A MnN4 moiety embedded graphene as a magnetic gas sensor for CO detection: A first principle study. *Appl. Surf. Sci.* **2019**, *473*, 820–827. [CrossRef]
4. Su, Y.; Xie, G.; Tai, H.; Li, S.; Yang, B.; Wang, S.; Zhang, Q.; Du, H.; Zhang, H.; Du, X.; et al. Self-powered room temperature NO_2 detection driven by triboelectric nanogenerator under UV illumination. *Nano Energy* **2018**, *47*, 316–324. [CrossRef]
5. Kim, D.-W.; Ha, S.; Ko, Y.-I.; Wee, J.-H.; Kim, H.J.; Jeong, S.Y.; Tojo, T.; Yang, C.-M.; Kim, Y.A. Rapid, repetitive and selective NO_2 gas sensor based on boron-doped activated carbon fibers. *Appl. Surf. Sci.* **2020**, *531*, 147395. [CrossRef]
6. Zhang, Z.; Gao, Z.; Fang, R.; Li, H.; He, W.; Du, C. UV-assisted room temperature NO_2 sensor using monolayer graphene dec-orated with SnO2 nanoparticles. *Ceram. Int.* **2020**, *46*, 2255–2260. [CrossRef]
7. Yang, Y.; Tian, C.; Wang, J.; Sun, L.; Shi, K.; Zhou, W.; Fu, H. Facile synthesis of novel 3D nanoflower-like CuxO/multilayer graphene composites for room temperature NOx gas sensor application. *Nanoscale* **2014**, *6*, 7369–7378. [CrossRef]
8. Novoselov, K.S.; Geim, A.K.; Morozov, S.V.; Jiang, D.; Zhang, Y.; Dubonos, S.V.; Grigorieva, I.V.; Firsov, A.A. Electric Field Effect in Atomically Thin Carbon Films. *Science* **2004**, *306*, 666–669. [CrossRef]
9. Wei, Q.; Sun, J.; Song, P.; Yang, Z.; Wang, Q. Synthesis of reduced graphene oxide/SnO_2 nanosheets/Au nanoparticles ternary composites with enhanced formaldehyde sensing performance. *Phys. E Low-Dimens. Syst. Nanostruct.* **2020**, *118*, 113953. [CrossRef]
10. Chen, Y.; Song, B.; Lu, L.; Xue, J. Ultra-small Fe_3O_4 nanoparticle decorated graphene nanosheets with superior cyclic perfor-mance and rate capability. *Nanoscale* **2013**, *5*, 6797–6803. [CrossRef]
11. You, X.; Yang, J.; Wang, M.; Wang, H.; Gao, L.; Dong, S. Interconnected graphene scaffolds for functional gas sensors with tunable sensitivity. *J. Mater. Sci. Technol.* **2020**, *58*, 16–23. [CrossRef]
12. Llobet, E. Gas sensors using carbon nanomaterials: A review. *Sens. Actuators B Chem.* **2013**, *179*, 32–45. [CrossRef]
13. Xiao, Z.; Kong, L.B.; Ruan, S.; Li, X.; Yu, S.; Li, X.; Jiang, Y.; Yao, Z.; Ye, S.; Wang, C.; et al. Recent development in nanocarbon materials for gas sensor applications. *Sens. Actuators B Chem.* **2018**, *274*, 235–267. [CrossRef]
14. Saleh, T.A.; Fadillah, G. Recent trends in the design of chemical sensors based on graphene–metal oxide nanocomposites for the analysis of toxic species and biomolecules. *TrAC Trends Anal. Chem.* **2019**, *120*, 115660. [CrossRef]
15. Chen, Y.; Song, B.; Chen, R.M.; Lu, L.; Xue, J. A study of the superior electrochemical performance of 3 nm SnO_2 nanoparticles supported by graphene. *J. Mater. Chem. A* **2014**, *2*, 5688–5695. [CrossRef]
16. Yan, K.; Fu, L.; Peng, H.; Liu, Z. Designed CVD Growth of Graphene via Process Engineering. *Accounts Chem. Res.* **2012**, *46*, 2263–2274. [CrossRef] [PubMed]
17. Yuan, Y.; Zhang, F.; Wang, H.; Liu, J.; Zheng, Y.; Hou, S. Chemical vapor deposition graphene combined with Pt nanoparticles applied in non-enzymatic sensing of ultralow concentrations of hydrogen peroxide. *RSC Adv.* **2017**, *7*, 30542–30547. [CrossRef]
18. Tromp, R.M.; Hannon, J.B. Thermodynamics and kinetics of graphene growth on SiC(0001). *Phys. Rev. Lett.* **2009**, *102*, 106104. [CrossRef]
19. Marcano, D.C.; Kosynkin, D.V.; Berlin, J.M.; Sinitskii, A.; Sun, Z.; Slesarev, A.; Alemany, L.B.; Lu, W.; Tour, J.M. Improved Synthesis of Graphene Oxide. *ACS Nano* **2010**, *4*, 4806–4814. [CrossRef]
20. Haridas, V.; Sukhananazerin, A.; Sneha, J.M.; Pullithadathil, B.; Narayanan, B. α-Fe_2O_3 loaded less-defective graphene sheets as chemiresistive gas sensor for selective sensing of NH3. *Appl. Surf. Sci.* **2020**, *517*, 146158. [CrossRef]
21. Song, H.; Li, X.; Cui, P.; Guo, S.; Liu, W.; Wang, X. Sensitivity investigation for the dependence of monolayer and stacking graphene NH_3 gas sensor. *Diam. Relat. Mater.* **2017**, *73*, 56–61. [CrossRef]
22. Li, G.; Shen, Y.; Zhou, P.; Hao, F.; Fang, P.; Wei, D.; Meng, D.; San, X. Design and application of highly responsive and selective rGO-SnO_2 nanocomposites for NO_2 monitoring. *Mater. Charact.* **2020**, *163*, 110284. [CrossRef]
23. Lee, H.-Y.; Heish, Y.-C.; Lee, C.-T. High sensitivity detection of nitrogen oxide gas at room temperature using zinc ox-ide-reduced graphene oxide sensing membrane. *J. Alloy. Compd.* **2019**, *773*, 950–954. [CrossRef]
24. Zhang, J.; Liu, X.; Neri, G.; Pinna, N. Nanostructured Materials for Room-Temperature Gas Sensors. *Adv. Mater.* **2016**, *28*, 795–831. [CrossRef] [PubMed]

25. Liu, J.; Wang, S.; Wang, Q.; Geng, B. Microwave chemical route to self-assembled quasi-spherical Cu_2O microarchitectures and their gas-sensing properties. *Sens. Actuators B Chem.* **2009**, *143*, 253–260. [CrossRef]
26. Jayawardena, S.; Siriwardena, H.D.; Rajapakse, R.; Kubono, A.; Shimomura, M. Fabrication of a quartz crystal microbalance sensor based on graphene oxide/TiO_2 composite for the detection of chemical vapors at room temperature. *Appl. Surf. Sci.* **2019**, *493*, 250–260. [CrossRef]
27. Shafiei, M.; Bradford, J.; Khan, H.; Piloto, C.; Wlodarski, W.; Li, Y.; Motta, N. Low-operating temperature NO_2 gas sensors based on hybrid two-dimensional SnS_2-reduced graphene oxide. *Appl. Surf. Sci.* **2018**, *462*, 330–336. [CrossRef]
28. Na, C.W.; Kim, J.-H.; Kim, H.-J.; Woo, H.-S.; Gupta, A.; Kim, H.-K.; Lee, J.-H. Highly selective and sensitive detection of NO_2 using rGO-In_2O_3 structure on flexible substrate at low temperature. *Sens. Actuators B Chem.* **2018**, *255*, 1671–1679. [CrossRef]
29. Bai, S.; Li, Q.; Han, N.; Zhang, K.; Tang, P.; Feng, Y.; Luo, R.; Li, D.; Chen, A. Synthesis of novel $BiVO_4$/Cu_2O heterojunctions for improving $BiVO_4$ towards NO_2 sensing properties. *J. Colloid Interface Sci.* **2020**, *567*, 37–44. [CrossRef]
30. Li, Q.; Han, N.; Zhang, K.; Bai, S.; Guo, J.; Luo, R.; Li, D.; Chen, A. Novel p-n heterojunction of $BiVO_4$/Cu_2O decorated with rGO for low concentration of NO_2 detection. *Sens. Actuators B Chem.* **2020**, *320*, 128284. [CrossRef]
31. Lu, W.-C.; Kumar, S.S.; Chen, Y.-C.; Hsu, C.-M.; Lin, H.-N. Au/Cu2O/ZnO ternary nanocomposite for low concentration NO_2 gas sensing at room temperature. *Mater. Lett.* **2019**, *256*, 126657. [CrossRef]
32. Ha, N.H.; Thinh, D.D.; Huong, N.T.; Phuong, N.H.; Thach, P.D.; Hong, H.S. Fast response of carbon monoxide gas sensors using a highly porous network of ZnO nanoparticles decorated on 3D reduced graphene oxide. *Appl. Surf. Sci.* **2018**, *434*, 1048–1054. [CrossRef]
33. Hong, H.S.; Phuong, N.H.; Huong, N.T.; Nam, N.H.; Hue, N.T. Highly sensitive and low detection limit of resistive NO_2 gas sensor based on a MoS_2/graphene two-dimensional heterostructures. *Appl. Surf. Sci.* **2019**, *492*, 449–454. [CrossRef]
34. Su, Y.; Xie, G.; Chen, J.; Du, H.; Zhang, H.; Yuan, Z.; Ye, Z.; Du, X.; Tai, H.; Jiang, Y. Reduced graphene oxide–polyethylene oxide hybrid films for toluene sensing at room temperature. *RSC Adv.* **2016**, *6*, 97840–97847. [CrossRef]
35. Zhou, Y.; Lin, X.; Wang, Y.; Liu, G.; Zhu, X.; Huang, Y.; Guo, Y.; Gao, C.; Zhou, M. Study on gas sensing of reduced graphene oxide/ZnO thin film at room temperature. *Sens. Actuators B Chem.* **2017**, *240*, 870–880. [CrossRef]
36. Zhang, J.; Liu, J.; Peng, Q.; Wang, A.X.; Li, Y. Nearly Monodisperse Cu_2O and CuO Nanospheres: Preparation and Applications for Sensitive Gas Sensors. *Chem. Mater.* **2006**, *18*, 867–871. [CrossRef]
37. Deng, S.; Tjoa, V.; Fan, H.M.; Tan, H.R.; Sayle, D.C.; Olivo, M.; Mhaisalkar, S.; Wei, J.; Sow, C.H. Reduced graphene oxide conjugated Cu_2O nanowire mesocrystals for high-performance NO2 gas sensor. *J. Am. Chem. Soc.* **2012**, *134*, 4905–4917. [CrossRef] [PubMed]
38. Meng, H.; Yang, W.; Ding, K.; Feng, L.; Guan, Y. Cu_2O nanorods modified by reduced graphene oxide for NH_3 sensing at room temperature. *J. Mater. Chem. A* **2015**, *3*, 1174–1181. [CrossRef]
39. Wang, L.; Zhang, R.; Zhou, T.; Lou, Z.; Deng, J.; Zhang, T. Concave Cu_2O octahedral nanoparticles as an advanced sensing material for benzene (C_6H_6) and nitrogen dioxide (NO_2) detection. *Sens. Actuators B Chem.* **2016**, *223*, 311–317. [CrossRef]
40. Shen, Y.; Tian, F.H.; Chen, S.; Ma, Z.; Zhao, L.; Jia, X. Density functional theory study on the mechanism of CO sensing on Cu_2O (111) surface: Influence of the pre-adsorbed oxygen atom. *Appl. Surf. Sci.* **2014**, *288*, 452–457. [CrossRef]
41. Xu, J.; Wu, L.; Liu, Y.; Zhang, J.; Liu, J.; Shu, S.; Kang, X.; Song, Q.; Liu, D.; Huang, F.; et al. NiO-rGO composite for supercapacitor electrode. *Surf. Interfaces* **2020**, *18*, 100420. [CrossRef]
42. Zhou, Y.; Wang, Y.; Guo, Y. Cuprous oxide nanowires/nanoparticles decorated on reduced graphene oxide nanosheets: Sensitive and selective H_2S detection at low temperature. *Mater. Lett.* **2019**, *254*, 336–339. [CrossRef]
43. Mogi, I.; Watanabe, K.; Motokawa, M. Magneto-electropolymerization of conducting polypyrrole. *Phys. B Condens. Matter* **1998**, *246-247*, 412–415. [CrossRef]
44. Bora, C.; Dolui, S. Fabrication of polypyrrole/graphene oxide nanocomposites by liquid/liquid interfacial polymerization and evaluation of their optical, electrical and electrochemical properties. *Polymer* **2012**, *53*, 923–932. [CrossRef]
45. Kim, D.-H.; Richardson-Burns, S.M.; Hendricks, J.L.; Sequera, C.; Martin, D.C. Effect of Immobilized Nerve Growth Factor on Conductive Polymers: Electrical Properties and Cellular Response. *Adv. Funct. Mater.* **2007**, *17*, 79–86. [CrossRef]
46. Pernaut, J.-M.; Reynolds, J.R. Use of Conducting Electroactive Polymers for Drug Delivery and Sensing of Bioactive Molecules. A Redox Chemistry Approach. *J. Phys. Chem. B* **2000**, *104*, 4080–4090. [CrossRef]
47. Wang, Y.; Cao, L.; Li, J.; Kou, L.; Huang, J.; Feng, Y.; Chen, S. Cu/Cu_2O@Ppy nanowires as a long-life and high-capacity anode for lithium ion battery. *Chem. Eng. J.* **2020**, *391*, 123597. [CrossRef]
48. Chen, Z.; Liang, Y.; Liu, A.; Zhang, Y.; Sui, Y.; Hu, S.; Li, J.; Kang, H.; Wang, S.; Zhao, S.; et al. One-step hydrothermal synthesis of three-dimensional structures of MoS_2/Cu_2S hybrids via a copper foam-assisted method. *Mater. Lett.* **2020**, *273*, 127928. [CrossRef]
49. Zhang, C.; Hao, R.; Liao, H.; Hou, Y. Synthesis of amino-functionalized graphene as metal-free catalyst and exploration of the roles of various nitrogen states in oxygen reduction reaction. *Nano Energy* **2013**, *2*, 88–97. [CrossRef]
50. Yan, X.-Y.; Tong, X.-L.; Zhang, Y.-F.; Han, X.-D.; Wang, Y.-Y.; Jin, G.-Q.; Qin, Y.; Guo, X.-Y. Cuprous oxide nanoparticles dis-persed on reduced graphene oxide as an efficient electrocatalyst for oxygen reduction reaction. *Chem. Commun.* **2012**, *48*, 1892–1894. [CrossRef] [PubMed]
51. Li, B.; Liu, T.; Hu, L.; Wang, Y. A facile one-pot synthesis of Cu_2O/RGO nanocomposite for removal of organic pollutant. *J. Phys. Chem. Solids* **2013**, *74*, 635–640. [CrossRef]

52. Yang, M.; Wang, Y.; Dong, L.; Xu, Z.; Liu, Y.; Hu, N.; Kong, E.S.-W.; Zhao, J.; Peng, C. Gas Sensors Based on Chemically Reduced Holey Graphene Oxide Thin Films. *Nanoscale Res. Lett.* **2019**, *14*, 1–8. [CrossRef] [PubMed]
53. Xu, Y.; Sheng, K.; Li, C.; Shi, G. Highly conductive chemically converted graphene prepared from mildly oxidized graphene oxide. *J. Mater. Chem.* **2011**, *21*, 7376–7380. [CrossRef]
54. Wang, H.; Robinson, J.T.; Li, X.; Dai, H. Solvothermal Reduction of Chemically Exfoliated Graphene Sheets. *J. Am. Chem. Soc.* **2009**, *131*, 9910–9911. [CrossRef]
55. Miankushki, H.N.; Sedghi, A.; Baghshahi, S. Facile and scalable fabrication of graphene/polypyrrole/MnOx/$Cu(OH)_2$ composite for high-performance supercapacitors. *J. Solid State Electrochem.* **2018**, *22*, 3317–3329. [CrossRef]
56. Chakravarty, A.; Bhowmik, K.; Mukherjee, A.; De, G. Cu_2O Nanoparticles Anchored on Amine-Functionalized Graphite Nanosheet: A Potential Reusable Catalyst. *Langmuir* **2015**, *31*, 5210–5219. [CrossRef]
57. Gao, Y.; Liu, L.-Q.; Zu, S.-Z.; Peng, K.; Zhou, D.; Han, B.-H.; Zhang, Z. The Effect of Interlayer Adhesion on the Mechanical Behaviors of Macroscopic Graphene Oxide Papers. *ACS Nano* **2011**, *5*, 2134–2141. [CrossRef]
58. Wang, Y.; Hu, N.; Zhou, Z.; Xu, D.; Wang, Z.; Yang, Z.; Wei, H.; Kong, E.S.-W.; Zhang, Y. Single-walled carbon nanotube/cobalt phthalocyanine derivative hybrid material: Preparation, characterization and its gas sensing properties. *J. Mater. Chem.* **2011**, *21*, 3779–3787. [CrossRef]
59. Sun, J.; Sun, L.; Han, N.; Chu, H.; Bai, S.; Shu, X.; Luo, R.; Chen, A. rGO decorated CdS/CdO composite for detection of low concentration NO_2. *Sens. Actuators B Chem.* **2019**, *299*, 126832. [CrossRef]
60. Mane, A.; Navale, S.; Sen, S.; Aswal, D.; Gupta, S.K.; Patil, V. Nitrogen dioxide (NO_2) sensing performance of p-polypyrrole/n-tungsten oxide hybrid nanocomposites at room temperature. *Org. Electron.* **2015**, *16*, 195–204. [CrossRef]
61. Xu, H.; Zhang, J.; Rehman, A.U.; Gong, L.; Kan, K.; Li, L.; Shi, K. Synthesis of NiO@CuO nanocomposite as high-performance gas sensing material for NO_2 at room temperature. *Appl. Surf. Sci.* **2017**, *412*, 230–237. [CrossRef]
62. Zhou, Y.; Li, X.; Wang, Y.; Tai, H.; Guo, Y. UV Illumination-Enhanced Molecular Ammonia Detection Based on a Ternary-Reduced Graphene Oxide–Titanium Dioxide–Au Composite Film at Room Temperature. *Anal. Chem.* **2018**, *91*, 3311–3318. [CrossRef]
63. Zhou, Y.; Gao, C.; Guo, Y. UV assisted ultrasensitive trace NO_2 gas sensing based on few-layer MoS_2 nanosheet-ZnO nanowire heterojunctions at room temperature. *J. Mater. Chem. A* **2018**, *6*, 10286–10296. [CrossRef]
64. Wang, Y.-D.; Wu, X.-H.; Zhou, Z.-L. A new type of semiconductor gas sensor based on the n+n combined structure. *Sens. Actuators B Chem.* **2001**, *73*, 216–220. [CrossRef]
65. Lu, G.; Ocola, L.E.; Chen, J. Gas detection using low-temperature reduced graphene oxide sheets. *Appl. Phys. Lett.* **2009**, *94*, 083111. [CrossRef]